ACS OMEGA

Open Access

http://pubs.acs.org/journal/acsodf

Article

From Simple Palladium(II) Monomers to 2D Heterometallic Sodium−Palladium(II) Coordination Networks with 2-Halonicotinates

Ivan Kodrin, Maricel Rodríguez, Nives Politeo, Željka Soldin, Igor Kerš, Tomislav Rončević, Vedrana Čikeš Čulić, Vesna Sokol, Fabio Doctorovich,* and Boris-Marko Kukovec*

Cite This: *ACS Omega* 2024, 9, 4111−4122

Read Online

ACCESS | Metrics & More | Article Recommendations | Supporting Information

ABSTRACT: The 2D heterometallic sodium−palladium(II) coordination polymers with 2-halonicotinates [2-chloropyridine-3-carboxylate (2-chloronicotinate), 2-Clnic$^-$ and 2-bromopyridine-3-carboxylate (2-bromonicotinate), 2-Brnic$^-$], $\{[Na_2(H_2O)_2(\mu\text{-}H_2O)_4PdCl_2(\mu\text{-}2\text{-}Clnic\text{-}N{:}O')_2]\}_n$ (**1**), and $\{[Na_2(H_2O)_2(\mu\text{-}H_2O)_4PdBr_2(\mu\text{-}2\text{-}Brnic\text{-}N{:}O')_2]\cdot 2H_2O\}_n$ (**2**) were prepared in aqueous solutions under the presence of $NaHCO_3$, while palladium(II) monomers with the neutral 2-chloronicotinic and 2-bromonicotinic acid ligands, $[PdCl_2(2\text{-}ClnicH\text{-}N)_2]\cdot 2DMF$ (**3**) and $[PdCl_2(2\text{-}BrnicH\text{-}N)_2]\cdot 2DMF$ (**4**), were prepared in DMF/water mixtures (DMF = *N*,*N*′-dimethylformamide). The zigzag chains of water-bridged sodium ions are in turn bridged by $[PdCl_2(2\text{-}Clnic)_2]^{2-}$ moieties in **1** or by $[PdBr_2(2\text{-}Brnic)_2]^{2-}$ moieties in **2**, leading to the formation of the infinite 2D coordination networks of **1** or **2**. The DFT calculations showed the halosubstituents type (Cl *vs* Br) does not have an influence on the formation of either *trans* or *cis* isomers. The *trans* isomers were found in all reported compounds; being more stable for about 10 to 15 kJ mol^{-1}. The 2D coordination networks **1** and **2** are more stabilized by the formation of Na−$O_{carboxylate}$ bonds, comparing to the stabilization of palladium(II) monomers **3** and **4** by hydrogen-bonding with DMF molecules. The difference in DFT calculated energy stabilization for **1** and **2** is ascribed to the type of halosubstituents and to the presence/absence of lattice water molecules in **1** and **2**. The compounds show no antibacterial activity toward reference strains of *Escherichia coli* and *Staphylococcus aureus* bacteria and no antiproliferative activity toward bladder (T24) and lung (A549) cancer cell lines.

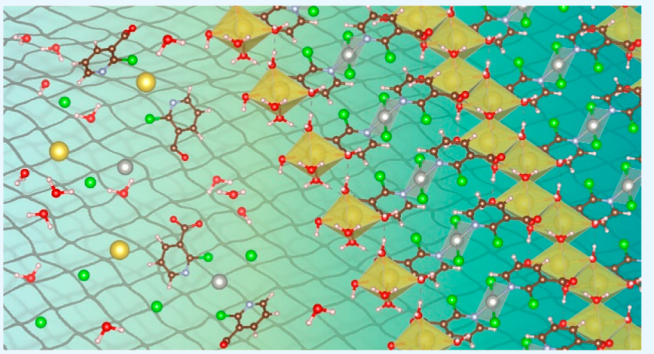

1. INTRODUCTION

Palladium(II) coordination compounds often show pronounced biological properties, *e.g.*, antitumor activity resembling cisplatin.[1,2] These complexes are usually kinetically more labile than their platinum(II) analogues in aqueous solutions,[3] causing their hydrolysis to be faster and enabling the hydrolyzed complexes to be more efficient in reaching pharmacological targets.[4,5] Hence, palladium(II) complexes could be better models for studying their interactions with the biologically important ligands *in vivo*. These interactions with target molecules, *e.g.*, tumor DNA, are crucial for the successful antitumor activity of palladium(II) complexes.[4] It is believed that a *cis*−*trans* isomerization of palladium(II) complexes in solution, promoted by a fast palladium(II) hydrolysis, hinders the antitumor efficiency of the usually active *cis* isomers.[6] Therefore, the synthetic protocols that would prevent palladium(II) complexes isomerization by the introduction of a strongly coordinated N atom from the main ligand (*e.g.*, nicotinate) and an appropriate leaving group (*e.g.*, halide ion) are of an increasing interest.[6] The coordinating ability of a donor N atom can be tuned by an induction of various electron-accepting or electron-donating substituents to the backbone of the main ligand (*e.g.*, nicotinate pyridine ring).

Heterometallic coordination polymers are an emerging class of compounds due to their enhanced properties and functionalities.[7] These coordination polymers contain different metal ions in a single framework, producing new cooperative and synergistic effects on their properties[8−12] and leading to new applications, *e.g.*, as heterogeneous catalysts in various organic reactions,[13,14] as luminescent compounds,[15] as heterogeneous electrocatalysts in reactions producing hydrogen and oxygen, in oxygen and carbon dioxide reduction, in

Received: November 28, 2023
Revised: December 21, 2023
Accepted: December 25, 2023
Published: January 11, 2024

various organic transformations, and in water splitting reactions.[16−24] In particular, palladium(II) coordination polymers and MOFs showed to be efficient catalysts for various reactions, probably due to a good dispersion of coordinatively unsaturated palladium(II) ions within the respective structures, increasing the catalytic activity.[25−27] The heterometallic coordination polymers are also often used as precursors in the production of inorganic materials, *e.g.*, various mixed-metal oxides, by precursors decomposition at high temperatures.[28−30]

The heterometallic sodium−palladium(II) coordination polymers with tridentate and chelating *N*-isopropyliminodiacetate and *N*-*tert*-butyliminodiacetate have been studied previously.[31] Both these ligands are coordinated to palladium(II) ions in a *N*,*O*,*O*′-tridentate fashion, while to sodium ions *via* other carboxylate O atoms, not coordinated to palladium(II) ion. It seems the *N*-isopropyl and *N*-*tert*-butyl substituents affect the dimensionality of the coordination polymers. The coordination polymer with *N*-isopropyliminodiacetate is 2D and the polymer with *N*-*tert*-butyliminodiacetate is 1D, most probably due to the bulkiness of the *N*-*tert*-butyl substituent.[31] The heterometallic alkali metal ion−palladium(II) coordination polymers with pyridinedicarboxylate are quite scarce in the literature. Only two such coordination polymers are known, *e.g.*, sodium−palladium(II) polymer with pyridine-2,6-dicarboxylate[32] and potassium−palladium(II) polymer with pyridine-2,3-dicarboxylate.[33] These two coordination polymers are rather similar; both pyridinedicarboxylates act as bidentate and bridging ligands *via* one of their carboxylate groups while the other is coordinated to the respective alkali metal ions, leading to the formation of 2D coordination networks.[32,33] The potassium−palladium polymer with pyridine-2,3-dicarboxylate exhibits good cytotoxic and antiproliferative activity *in vitro* toward various human tumor cells by cleaving the plasmid DNA of tumor cells.[33]

Our goal was to prepare heterometallic sodium−palladium(II) coordination polymers by using structurally simpler ligands than the said pyridinedicarboxylic acids, *e.g.*, monocarboxylic 2-halonicotinic acids [2-chloropyridine-3-carboxylic (2-chloronicotinic) acid, 2-ClnicH and 2-bromopyridine-3-carboxylic (2-bromonicotinic) acid, 2-BrnicH]. These ligands definitely cannot act as either bidentate and chelating (similar to pyridinedicarboxylates) or tridentate and chelating (similar to iminodiacetates), but exhibit solely a bridging potential *via* pyridine N and carboxylate O atoms. According to the hard−soft acid−base (HSAB) principle,[34] it is expected that N atoms will be coordinated to palladium(II) ions and O atoms to sodium ions. Since the halonicotinates can coordinate to palladium(II) ion only monodentately *via* N atom, the anticipated square-planar palladium(II) coordination environment will be probably completed by chloride ions (a suitable leaving group). Such coordination environment, preventing possible *cis*−*trans* isomerization upon hydrolysis in the aqueous solutions, makes these palladium(II) compounds to be ideal candidates for studying antitumor activity. Furthermore, we wanted to explore experimental conditions under which these sodium−palladium(II) coordination polymers can be obtained, *e.g.*, in aqueous solution in the presence of a base, *e.g.*, sodium bicarbonate or in the mixture of DMF and water. The carboxylic group will certainly deprotonate in the presence of the base and likely not deprotonate in the DMF/water mixture. Thus, we wanted to check if the halonicotinic acid/halonicotinate equilibrium has any effect on the formation of the desired coordination polymers. Lastly, we wanted to study the effect of the halosubstituent type (chloride *vs* bromide) in the same position (2-) on the pyridine ring, not only on the ability of the formation of the desired coordination polymers, but also on their dimensionality (1D *vs* 2D polymers). Since the antitumor properties of palladium(II) coordination compounds usually depend on the *cis* or *trans* arrangement of ligating atoms around palladium(II) ions, we wanted to determine if the choice of the halosubstituents type has any effect on the preferred formation of either *cis* or *trans* isomers, related to the potential antitumor activity.

In line with the stated objectives, we have prepared 2D heterometallic sodium−palladium(II) coordination polymers with 2-halonicotinates (2-Clnic$^-$ and 2-Brnic$^-$), $\{[Na_2(H_2O)_2(\mu\text{-}H_2O)_4PdCl_2(\mu\text{-}2\text{-Clnic-}N{:}O')_2]\}_n$ (**1**) and $\{[Na_2(H_2O)_2(\mu\text{-}H_2O)_4PdBr_2(\mu\text{-}2\text{-Brnic-}N{:}O')_2]\cdot 2H_2O\}_n$ (**2**), and palladium(II) monomers with the neutral 2-chloronicotinic and 2-bromonicotinic acid ligands, $PdCl_2(2\text{-ClnicH-}N)_2]\cdot 2DMF$ (**3**) and $[PdCl_2(2\text{-BrnicH-}N)_2]\cdot 2DMF$ (**4**). The experimental findings were rationalized by DFT calculations. The antibacterial properties of all the compounds were tested against Gram-negative and Gram-positive bacteria whereas antitumor activity was assessed against bladder and lung cancer cell lines.

2. EXPERIMENTAL SECTION

2.1. Materials and Physical Measurements. The commercially available chemicals used for the syntheses were of a reagent grade, used as received from commercial sources Alfa Aesar, Sigma-Aldrich or TCI Europe N. V. and were not purified further. The CHN elemental analyses were carried out with a PerkinElmer 2400 Series II CHNS analyzer in the Analytical Services Laboratories of the Ruđer Bošković Institute, Zagreb, Croatia. The IR spectra (Figures S1−S4) were obtained from KBr pellets in the range 4000−400 cm^{-1} on a Bruker Alpha II FT-IR spectrometer. The solution-state NMR spectra (Figures S5−S16) were recorded on a Bruker Avance III HD 400 MHz NMR spectrometer at 25.0 °C. DMSO-d_6 was used as solvent and TMS as an internal standard for chemical shifts. The NMR spectra of free ligands 2-BrnicH and 2-ClnicH were recorded for comparison with chemical shifts of coordinated ligands in compounds **1**−**4**. Thermogravimetric analysis was performed using a simultaneous TGA/DSC analyzer Mettler-Toledo TGA/DSC 3+. The samples of compounds **1**−**4** were placed in alumina pans (70 μL), heated in flowing nitrogen (50 mL min^{-1}) from room temperature up to 1000 °C at a rate of 10 °C min^{-1}. Data collection and analysis were performed using the program package STARe Software 15.01 MettlerToledo GmbH, 2015. Powder X-ray diffraction experiments (PXRD) were measured on a Malvern Panalytical Aeris XRD diffractometer with Cu Kα (1.5406 Å) radiation, Ni filter, and solid-state PIXcel1D-Medipix3 detector. Samples were prepared as a thin layer on a silicon zero-background plate. Data were collected in the 2θ range from 5 to 40° with a step size of 0.02173°, scan rate 10 s/°, 1/4 in. divergence slit and 13 mm beam mask.

2.2. Syntheses. *2.2.1.* $\{[Na_2(H_2O)_2(\mu\text{-}H_2O)_4PdCl_2(\mu\text{-}2\text{-Clnic-}N{:}O')_2]\}_n$ *(**1**).* 2-Chloropyridine-3-carboxylic acid (0.0500 g, 0.3174 mmol) was dissolved in 2 mL of distilled water, sodium tetrachloropalladate(II) (0.0474 g, 0.1611 mmol) was dissolved in 1 mL of distilled water, and sodium bicarbonate (0.0477 g, 0.5678 mmol) was dissolved in 1 mL of distilled water. The solutions of 2-chloropyridine-3-carboxylic

https://doi.org/10.1021/acsomega.3c09497
ACS Omega 2024, 9, 4111−4122

Table 1. Crystallographic Data for 1−4

compound	1	2	3	4
formula	$C_{12}H_{18}PdCl_4Na_2N_2O_{10}$	$C_{12}H_{22}PdBr_4Na_2N_2O_{12}$	$C_{18}H_{22}PdCl_4N_4O_6$	$C_{18}H_{22}PdBr_2Cl_2N_4O_6$
M_r	644.46	858.33	638.59	727.51
crystal system, space group	triclinic, $P\bar{1}$ (no. 2)	triclinic, $P\bar{1}$ (no. 2)	triclinic, $P\bar{1}$ (no. 2)	monoclinic, $P2_1/n$ (no. 14)
a (Å)	5.5372(4)	5.5727(3)	6.3841(5)	6.0561(2)
b (Å)	7.8913(4)	8.3432(5)	8.3491(6)	30.9525(11)
c (Å)	14.5355(6)	14.7679(6)	11.8775(9)	7.3207(3)
α (deg)	81.921(4)	91.411(4)	90.663(6)	90
β (deg)	79.484(4)	99.035(4)	99.561(6)	112.432(4)
γ (deg)	70.694(5)	107.763(5)	98.092(7)	90
V (Å^3)	587.15(6)	643.85(6)	617.68(8)	1268.44(9)
Z	1	1	1	2
D_{calc} (g cm^{-3})	1.823	2.214	1.717	1.905
μ (mm^{-1})	11.397	7.016	10.411	11.893
R [$I \geq 2\sigma(I)$]	0.0336	0.0579	0.0698	0.0474
wR [all data]	0.0805	0.1808	0.1948	0.1224

acid and sodium bicarbonate were mixed and then slowly added to the sodium tetrachloropalladate(II) solution and stirred. The resulting solution was left to slowly evaporate at room temperature for a month. The obtained yellow crystals were collected by filtration, washed with water, and dried in air. Yield: 0.0304 g (29%, based on Na_2PdCl_4). Anal. Calcd for $C_{12}H_{18}PdCl_4Na_2N_2O_{10}$: C, 22.36; H, 2.82; N, 4.35. Found: C, 22.24; H, 2.85; N, 4.40.

IR (KBr pellet, cm^{-1}): 3494(m), 3300(w), 3213(w), 3062(w), 1723(w), 1658(m), 1612(s), 1583(m), 1449(w), 1411(m), 1389(s), 1248(w), 1225(w), 1174(w), 1137(w), 1109(w), 1064(w), 865(w), 834(w), 783(w), 747(w), 698(w), 669(w), 557(w), 541(w), 510(w), 483(w), 450(w), 411(w).

^{1}H NMR (DMSO-d_6, 400 MHz): δ (ppm) 8.20 (dd, 1H, J = 4.7 and 2.0 Hz, H6), 7.74 (dd, 1H, J = 7.4 and 1.8 Hz, H4), 7.29 (dd, 1H, J = 7.4 and 4.7 Hz, H5).

^{13}C NMR (DMSO-d_6, 100 MHz): δ (ppm) 168.6 (C7), 147.4 (C6), 146.7 (C2), 139.3 (C3), 137.6 (C5), 123.1 (C4).

*2.2.2. {[$Na_2(H_2O)_2(\mu$-$H_2O)_4PdBr_2(\mu$-2-Brnic-N:O′)$_2$]·2H_2O}$_n$ (**2**).* The similar procedure was employed as for the preparation of **1**; 2-bromopyridine-3-carboxylic acid (0.0495 g, 0.2450 mmol), sodium tetrachloropalladate(II) (0.0375 g, 0.1275 mmol), and sodium bicarbonate (0.0516 g, 0.6142 mmol) were used. Yield: 0.0257 g (23%, based on Na_2PdCl_4). Anal. Calcd for $C_{12}H_{22}PdBr_4Na_2N_2O_{12}$: C, 16.79; H, 2.59; N, 3.26. Found: C, 16.62; H, 2.63; N, 3.31.

IR (KBr pellet, cm^{-1}): 3475(s), 3243(m), 3061(m), 2257(w), 2122(w), 1982(w), 1776(w), 1657(m), 1610(s), 1579(m), 1447(w), 1392(s), 1244(w), 1218(w), 1170(w), 1127(w), 1098(m), 1053(w), 994(w), 863(w), 829(w), 780(m), 723(m), 694(m), 669(m), 599(w), 521(w), 418(w).

^{1}H NMR (DMSO-d_6, 400 MHz): δ (ppm) 8.15 (dd, 1H, J = 4.6 and 1.9 Hz, H6), 7.64 (d, 1H, J = 7.4 Hz, H4), 7.30 (dd, 1H, J = 7.4 and 4.7 Hz, H5).

^{13}C NMR (DMSO-d_6, 100 MHz): δ (ppm) 169.1 (C7), 147.8 (C6), 142.3 (C2), 138.5 (C3), 136.9 (C5), 123.3 (C4).

*2.2.3. [$PdCl_2$(2-ClnicH-N)$_2$]·2DMF (**3**).* 2-Chloropyridine-3-carboxylic acid (0.2004 g, 1.2720 mmol) was dissolved in 3 mL of *N*,*N*′-dimethylformamide and sodium tetrachloropalladate-(II) (0.1866 g, 0.6342 mmol) was dissolved in 3 mL of distilled water. The solution of 2-chloropyridine-3-carboxylic acid was slowly added to the sodium tetrachloropalladate(II) solution and stirred. The resulting solution was left to slowly evaporate at room temperature for 1 day. The obtained yellow precipitate was collected by filtration, washed with the DMF/water mixture (1:1, V/V), and dried in air. Yield: 0.2942 g (73%, based on Na_2PdCl_4). Anal. Calcd for $C_{18}H_{22}PdCl_4N_4O_6$: C, 33.85; H, 3.48; N, 8.78. Found: C, 33.76; H, 3.52; N, 8.83.

IR (KBr pellet, cm^{-1}): 3475(m), 3430(m), 3087(w), 3066(w), 3001(w), 2963(w), 2926(w), 2800(w), 2637(w), 2521(w), 2236(w), 1919(w), 1707(s), 1625(m), 1585(s), 1478(w), 1411(s), 1371(m), 1291(s), 1162(w), 1105(m), 1067(w), 1013(w), 863(w), 832(m), 765(m), 731(w), 677(m), 564(w), 503(w), 485(w), 411(w).

^{1}H NMR (DMSO-d_6, 400 MHz): δ (ppm) 8.55 (d, 1H, J = 3.2 Hz, H6), 8.22 (d, 1H, J = 6.8 Hz, H4), 7.95 (s, 1H, CH-DMF), 7.54 (dd, 1H, J = 7.4 and 4.8 Hz, H5), 2.89 (s, 3H, CH_3-DMF), 2.73 (s, 3H, CH_3-DMF).

^{13}C NMR (DMSO-d_6, 100 MHz): δ (ppm) 166.2 (C7), 162.8 (CH-DMF), 152.2 (C6), 148.2 (C2), 140.5 (C5), 128.6 (C3), 123.6 (C4), 36.3 (CH_3-DMF), 31.2 (CH_3-DMF).

The preparation of single crystals: 2-chloropyridine-3-carboxylic acid (0.0500 g, 0.3174 mmol) was dissolved in 3 mL of *N*,*N*′-dimethylformamide, sodium tetrachloropalladate-(II) (0.0461 g, 0.1567 mmol) in 3 mL of distilled water, and the two solutions were mixed. The resulting solution was left to slowly evaporate at room temperature for 2 days. The obtained yellow crystals, suitable for X-ray crystal structure determination, were collected by filtration and dried in air. Yield: 0.0570 g (57%, based on Na_2PdCl_4).

*2.2.4. [$PdCl_2$(2-BrnicH-N)$_2$]·2DMF (**4**).* A similar procedure was employed as for the preparation of **3**; 2-bromopyridine-3-carboxylic acid (0.2006 g, 0.9930 mmol) and sodium tetrachloropalladate(II) (0.1463 g, 0.4973 mmol) were used. Yield: 0.2470 g (68%, based on Na_2PdCl_4). Anal. Calcd for $C_{18}H_{22}PdBr_2Cl_2N_4O_6$: C, 29.72; H, 3.05; N, 7.70. Found: C, 29.62; H, 3.09; N, 7.76.

IR (KBr pellet, cm^{-1}): 3504(m), 3434(w), 3393(w), 3069(w), 3004(w), 2972(w), 2927(w), 2785(w), 2627(w), 2507(w), 2258(w), 1928(w), 1719(s), 1640(m), 1585(s), 1484(w), 1410(m), 1372(m), 1291(s), 1162(w), 1127(w), 1097(m), 1059(w), 1013(w), 931(w), 868(w), 829(m), 766(m), 707(w), 682(m), 579(w), 561(w), 532(w), 481(w), 449(w), 408(w).

^{1}H NMR (DMSO-d_6, 400 MHz): δ (ppm) 8.51 (d, 1H, J = 4.2 Hz, H6), 8.13 (d, 1H, J = 7.4 Hz, H4), 7.95 (s, 1H, CH-DMF), 7.55 (dd, 1H, J = 7.4 and 4.8 Hz, H5), 2.89 (s, 3H, CH_3-DMF), 2.73 (s, 3H, CH_3-DMF).

https://doi.org/10.1021/acsomega.3c09497
ACS Omega 2024, 9, 4111−4122

^{13}C NMR (DMSO-d_6, 100 MHz): δ (ppm) 166.9 (C7), 162.8 (CH-DMF), 152.4 (C6), 139.7 (C5), 139.2 (C2), 131.6 (C3), 123.6 (C4), 36.3 (CH_3-DMF), 31.2 (CH_3-DMF).

The single crystals were prepared as in the case of single crystals of **3**; 2-bromopyridine-3-carboxylic acid (0.0500 g, 0.2475 mmol) and sodium tetrachloropalladate(II) (0.0364 g, 0.1237 mmol) were used. Yield: 0.0434 g (48%, based on Na_2PdCl_4).

2.3. X-ray Crystallographic Analysis. The suitable single crystals of **1**−**4** were selected and mounted onto cryoloops. The data collection was carried out on an Oxford Diffraction-Rigaku Xcalibur Gemini E four-circle kappa geometry diffractometer with Eos CCD detector, using graphite monochromated Cu Kα (λ = 1.54184 Å) radiation for **1**, **3**, and **4** or Mo Kα (λ = 0.71073 Å) radiation for **2** at room temperature [296(2) K] and by applying the CrysAlis PRO Software system.[35] The data reduction and cell refinement were performed by the CrysAlis PRO Software system.[35] The structures were solved by SHELXT-2018/2[36] and refined by SHELXL-2018/3.[37] The refinement procedure was done by full-matrix least-squares methods based on F^2 values against all reflections. The figures were made with MERCURY (Version 2023.2.0).[38] The crystallographic data for **1**−**4** are summarized in Table 1.

2.4. Computational Details. Periodic density functional theory (DFT) calculations were performed in CRYSTAL17.[39] PBE functional[40] were used and Grimme's D3 correction[41] was included for a better description of the weak dispersive interactions. Triple-zeta basis set pob-TZVP-rev2, adapted for periodic calculations, was employed for all atoms.[42] The input files for CRYSTAL17 were created from CIF files with cif2cell.[43] Full optimization was performed with default convergence criteria. Total energy convergence was set to 10^{-7} and truncation criteria for the calculations of Coulomb and exchange integrals increased to (8 8 8 8 16) for SCF calculations. Molecules were visualized in VESTA.[44] Interaction energies E_{int} were calculated according to formula $E_{A\cdots B} - (E_A + E_B)$, where $E_{A\cdots B}$ is the energy of a fully optimized unit cell with both fragments A and B, and E_A and E_B are basis set superposition error (BSSE) corrected single point energies of individual fragments A and B with the same geometry and the same arrangement of molecules as in the optimized unit cell.[45]

2.5. Antimicrobial Activity. The antibacterial *in vitro* testing was performed on *Escherichia coli* ATCC 25922 and *Staphylococcus aureus* ATCC 29213 as representatives of Gram-negative and Gram-positive bacteria, respectively. Activity of the compounds **1**−**4** was assessed using the 2-fold micro-dilution method and performed in 96-well microtiter plates as previously described.[46] Briefly, overnight grown bacteria were cultured in fresh Mueller Hinton broth to the mid exponential phase. These were then added to serial dilutions of the complexes (0.125−128 μg mL^{-1}) to a final bacterial load of 5 × 10^5 CFU mL^{-1} in 100 μL per well. The suspension was incubated at 37 °C for 18−20 h and minimum inhibitory concentration (MIC) was taken as the lowest concentration of the complex showing no visually detectable bacterial growth.

2.6. Antiproliferative Activity. The antiproliferative activity of compounds **1**−**4** was investigated against the human bladder cancer cell line T24 and human lung cancer cell line A549. Cells were grown in Dulbecco's modified Eagle's medium (DMEM, Euroclone, Milano, Italy) in a humidified incubator at 37 °C with 5% CO_2. The complete DMEM medium contained 10% fetal bovine serum (FBS, Euroclone, Milano, Italy) and 1% antibiotics (penicillin and streptomycin, Euroclone, Milano, Italy). The equal number of cells (1 × 10^4) were transferred into 96 wells and left overnight. Next day, the cells were treated with tested compounds for 4, 24, 48, and 72 h at a concentration of 1, 5, 10, 50, and 100 μg mL^{-1}. Three wells per plate were used as a control and incubated in complete medium.

Cell proliferation was determined using MTT [3-(4,5-dimethylthiazolid-2)-2,5-diphenyltetrazoline bromide] assay. Yellow tetrazoline MTT is reduced in metabolically active cells to the purple formazan. After 4, 24, 48, or 72 h of incubation with the samples, MTT was added to all wells and incubated for 2 h at 37 °C. Then, the medium with MTT was removed and DMSO was added. The plates were incubated for 10 min at 37 °C with shaking. The absorbance was measured at 570 nm with microplate photometer HiPo MPP-96 (Biosan, Riga, Latvia). All measurements were carried out in triplicate and the obtained results were expressed as percentage of treated live cells over nontreated cells (control).

For statistical analyses, *t*-test with unequal variances was performed using statistical software GraphPad Prism 8.0 (San Diego, CA, USA) with the significance set at $P < 0.5$. The calculation of IC_{50} values was performed with the GraphPad Prism software version 8.0 (San Diego, CA, USA), normalizing the data by three independent measurements of untreated controls.

3. RESULTS AND DISCUSSION

3.1. Syntheses Aspects. The 2D heterometallic sodium−palladium(II) coordination polymers, $\{[Na_2(H_2O)_2(\mu\text{-}H_2O)_4PdCl_2(\mu\text{-}2\text{-}Clnic\text{-}N{:}O')_2]\}_n$ (**1**) and $\{[Na_2(H_2O)_2(\mu\text{-}H_2O)_4PdBr_2(\mu\text{-}2\text{-}Brnic\text{-}N{:}O')_2]\cdot 2H_2O\}_n$ (**2**), were prepared by the reactions of sodium tetrachloropalladate(II), 2-chloronicotinic (for **1**) or 2-bromonicotinic (for **2**) acid and sodium bicarbonate (molar ratio 1:2:4) in aqueous solutions. The palladium(II) monomers, $PdCl_2(2\text{-}ClnicH\text{-}N)_2]\cdot 2DMF$ (**3**) and $[PdCl_2(2\text{-}BrnicH\text{-}N)_2]\cdot 2DMF$ (**4**), were prepared by the reactions of sodium tetrachloropalladate(II) and 2-chloronicotinic (for **3**) or 2-bromonicotinic (for **4**) acid (molar ratio 1:2) in DMF/water mixtures (1:1, V/V) (Scheme 1).

Scheme 1. Preparation of $\{[Na_2(H_2O)_2(\mu\text{-}H_2O)_4PdCl_2(\mu\text{-}2\text{-}Clnic\text{-}N{:}O')_2]\}_n$ (1), $\{[Na_2(H_2O)_2(\mu\text{-}H_2O)_4PdBr_2(\mu\text{-}2\text{-}Brnic\text{-}N{:}O')_2]\cdot 2H_2O\}_n$ (2), $[PdCl_2(2\text{-}ClnicH\text{-}N)_2]\cdot 2DMF$ (3), and $[PdCl_2(2\text{-}BrnicH\text{-}N)_2]\cdot 2DMF$ (4)

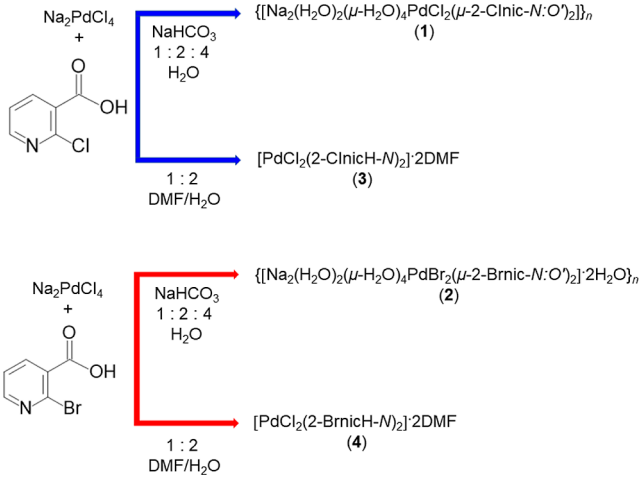

https://doi.org/10.1021/acsomega.3c09497
ACS Omega 2024, 9, 4111−4122

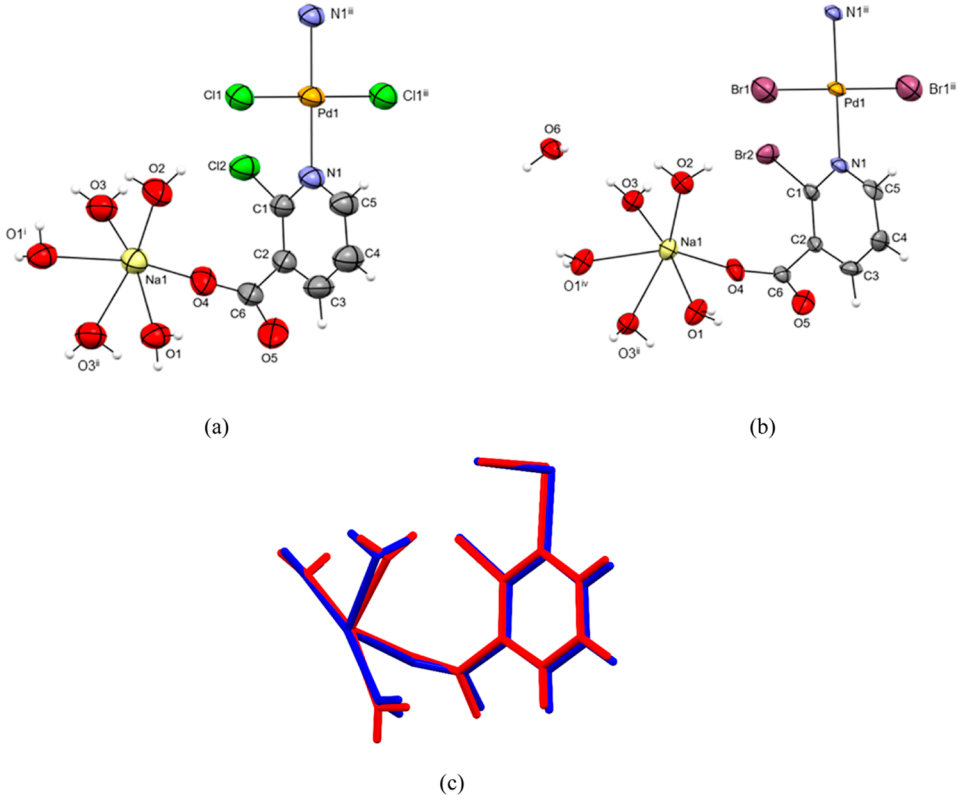

Figure 1. ORTEP-style plots of $\{[Na_2(H_2O)_2(\mu\text{-}H_2O)_4PdCl_2(\mu\text{-}2\text{-Clnic-}N{:}O')_2]\}_n$ (**1**) (a) and $\{[Na_2(H_2O)_2(\mu\text{-}H_2O)_4PdBr_2(\mu\text{-}2\text{-Brnic-}N{:}O')_2]\cdot 2H_2O\}_n$ (**2**) (b) with the corresponding atomic numbering schemes [symmetry codes (i): $-x + 2, -y + 1, -z$; (ii): $-x + 1, -y + 1, -z$; (iii): $-x + 1, -y + 1, -z + 1$; (iv): $-x, -y + 1, -z$]. Thermal ellipsoids are drawn at the 50% probability level at 296(2) K and hydrogen atoms are shown as spheres of arbitrary radii. Overlay (RMS value of 0.216 Å) of the asymmetric units of **1** (red) and **2** (blue); the lattice water molecule in **2** is omitted. The Pd, Na, N, O, and halide atoms were chosen for the overlay (c).

3.2. Crystal Structures. As palladium(II) ions are placed on an inversion center in both **1** and **2**, the asymmetric unit of **1** is composed of a palladium(II) ion, a coordinated chloride ion, a coordinated 2-chloronicotinate ion, a sodium ion, and three coordinated water molecules (Figure 1a), while the asymmetric unit of **2** is composed of a palladium(II) ion, a coordinated bromide ion, a coordinated 2-bromonicotinate ion, a sodium ion, three coordinated water molecules, and a lattice water molecule (Figure 1b). The overlay of the asymmetric units of **1** and **2** is shown in Figure 1c. Each of the palladium(II) ions in **1** and **2** is coordinated with two halide ions (Cl1 and $Cl1^{iii}$ in **1** or Br1 and $Br2^{iii}$ in **2**) and two pyridine N atoms (N1 and $N1^{iii}$) in *trans* position ($N1^{iii}$–Pd1–N1, 180°; symmetry code (iii): $-x + 1, -y + 1, -z + 1$), resulting in a square-planar coordination environment (Figure 1a,b and Table S1) with τ_4 value[47] of 0 for both **1** and **2**. The palladium(II) square-planar coordination environments are not distorted, as the bond angles around palladium(II) ions have almost ideal values (Table S1). Each of the sodium ions in **1** and **2** is octahedrally coordinated with four bridging water molecules [O1, $O1^{i}$ (in **1**) or $O1^{iv}$ (in **2**), O3, and $O3^{ii}$ atoms; symmetry codes (i): $-x + 2, -y + 1, -z$; (ii): $-x + 1, -y + 1, -z$; (iv): $-x, -y + 1, -z$] and with the carboxylate O4 atom and terminal water molecule (O2 atom) in *cis* position [O4–Na1–O2, 113.1(1)° (in **1**) or 117.0(3)° (in **2**), Figure 1a,b and Table S1]. The sodium coordination environments are distorted due to the high number of bridging water molecules, as indicated by *trans* [a range of 158.6(1)–166.2(1)° in **1** and 153.8(3)–168.1(3)° in **2**] and *cis* pairs [a range of 79.5(1)–113.1(1)° in **1** and 71.6(2)–117.0(3)° in **2**] of ligating atoms around sodium ions (Table S1). The square planes around palladium(II) (defined by Cl1/N1/$Cl1^{iii}$/$N1^{iii}$ atoms in **1** or Br1/N1/$Br1^{iii}$/$N1^{iii}$ atoms in **2**) are almost perpendicular to the corresponding pyridine rings defined by N1/C1/C2/C3/C4/C5 atoms [87.5(2)° in **1** and 81.5(3)° in **2**].

The 2-chloronicotinate and 2-bromonicotinate ligands both act as *N:O′*-bridging between the adjacent palladium(II) and sodium ions, binding to the palladium(II) ion *via* their pyridine N atom and to the sodium ion *via* their carboxylate O atom. The $[PdCl_2(2\text{-Clnic})_2]^{2-}$ (in **1**) or $[PdBr_2(2\text{-Brnic})_2]^{2-}$ (in **2**) moieties and sodium ions are the main building units of the coordination polymers **1** and **2**, respectively (Figure 2a,b). Each $[PdCl_2(2\text{-Clnic})_2]^{2-}$ or $[PdBr_2(2\text{-Brnic})_2]^{2-}$ moiety is coordinated to two neighboring sodium ions, while each sodium ion is connected to two neighboring sodium ions; to each of them *via* two bridging water molecules [*e.g.*, to the one of the neighboring sodium ions *via* O1 and $O1^{i}$ (in **1**) or $O1^{iv}$ (in **2**) atoms and to the other sodium ion *via* O3 and $O3^{ii}$ atoms], resulting in the formation of the nearly perpendicular four-membered rings [the ring Na1/O1/$Na1^{i}$/$O1^{i}$ (in **1**) or Na1/O1/$Na1^{iv}$/$O1^{iv}$ (in **2**) being almost perpendicular to the ring Na1/O3/$Na1^{ii}$/$O3^{ii}$; 79.2(1)° in **1** and 72.0(3)° in **2**]. In this way, the water-bridged sodium ions are connected into a zigzag chain along the [100] direction. These symmetry-related sodium zigzag chains are in turn bridged by $[PdCl_2(2\text{-Clnic})_2]^{2-}$ moieties along the [001] direction in **1** or by $[PdBr_2(2\text{-Brnic})_2]^{2-}$ moieties along the [−101] direction in **2**, leading to the formation of the infinite 2D coordination

https://doi.org/10.1021/acsomega.3c09497
ACS Omega 2024, 9, 4111−4122

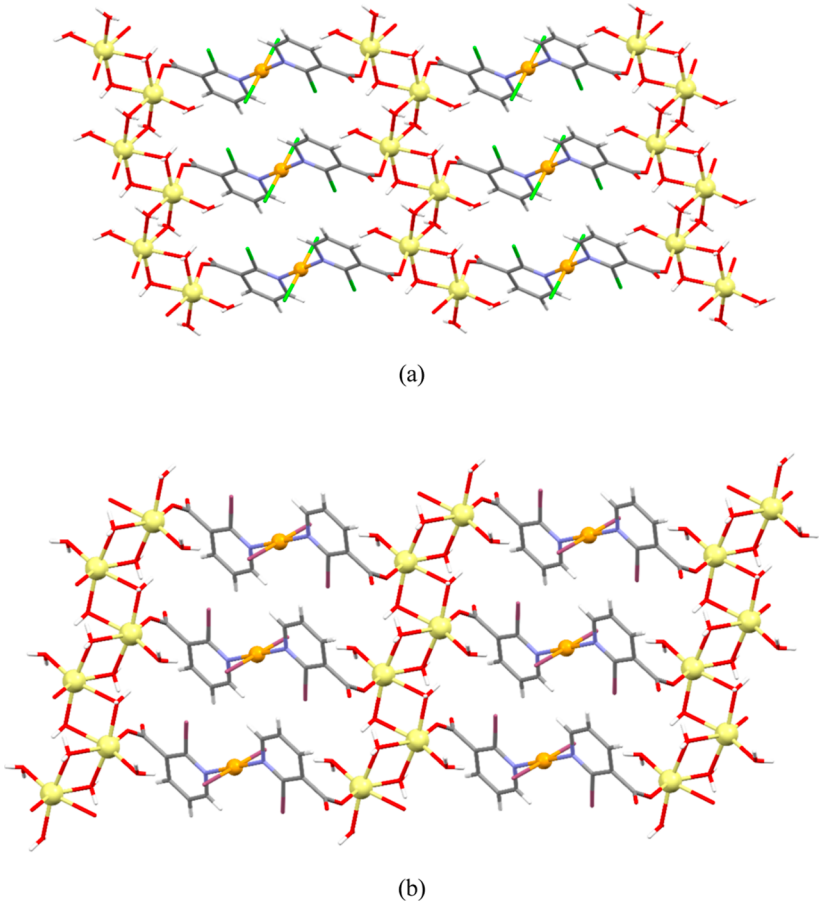

Figure 2. Infinite 2D coordination networks [parallel to the (010) plane] of $\{[Na_2(H_2O)_2(\mu\text{-}H_2O)_4PdCl_2(\mu\text{-}2\text{-}Clnic\text{-}N{:}O')_2]\}_n$ (**1**) (a) and $\{[Na_2(H_2O)_2(\mu\text{-}H_2O)_4PdBr_2(\mu\text{-}2\text{-}Brnic\text{-}N{:}O')_2]\cdot 2H_2O\}_n$ (**2**) (b); the water-bridged sodium ions are connected into a zigzag chain along the [100] direction and these chains are in turn bridged by $[PdCl_2(2\text{-}Clnic)_2]^{2-}$ along the [001] direction in **1** (a) or by $[PdBr_2(2\text{-}Bnic)_2]^{2-}$ moieties along the [−101] direction in **2** (b) (the lattice water molecules in **2** are not shown).

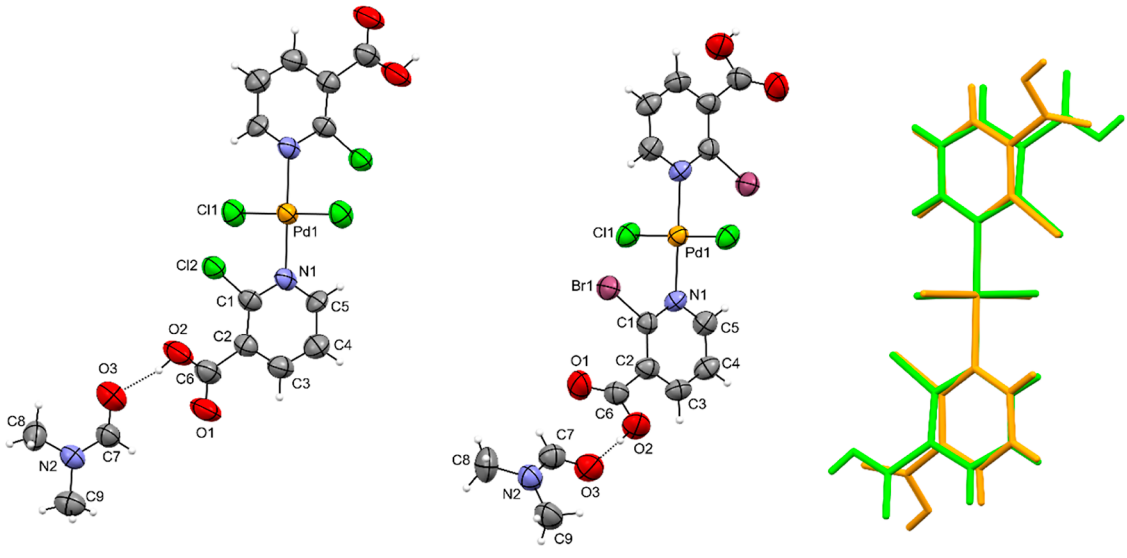

Figure 3. ORTEP-style plots of $[PdCl_2(2\text{-}ClnicH\text{-}N)_2]\cdot 2DMF$ (**3**) (a) and $[PdCl_2(2\text{-}BrnicH\text{-}N)_2]\cdot 2DMF$ (**4**) (b) with the corresponding atomic numbering schemes of the asymmetric units. Thermal ellipsoids are drawn at the 50% probability level at 296(2) K and hydrogen atoms are shown as spheres of arbitrary radii. Overlay (RMS value of 0.187 Å) of molecules of **3** (green) and **4** (orange); the lattice DMF molecules are omitted. The Pd, N, and halide atoms were chosen for the overlay (c).

https://doi.org/10.1021/acsomega.3c09497
ACS Omega 2024, 9, 4111−4122

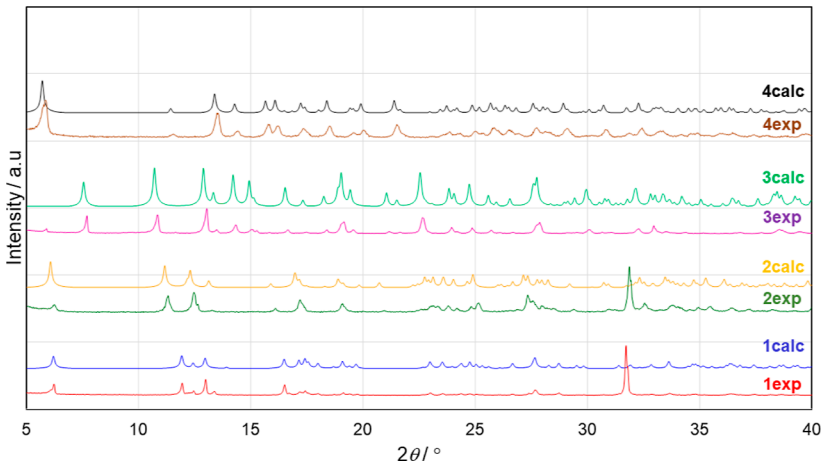

Figure 4. Overlay of the experimental and calculated PXRD traces of $\{[Na_2(H_2O)_2(\mu\text{-}H_2O)_4PdCl_2(\mu\text{-2-Clnic-}N{:}O')_2]\}_n$ (**1**), $\{[Na_2(H_2O)_2(\mu\text{-}H_2O)_4PdBr_2(\mu\text{-2-Brnic-}N{:}O')_2]\cdot 2H_2O\}_n$ (**2**), $[PdCl_2(\text{2-ClnicH-}N)_2]\cdot 2DMF$ (**3**), and $[PdCl_2(\text{2-BrnicH-}N)_2]\cdot 2DMF$ (**4**).

networks of **1** or **2**, parallel to the (010) plane. There are 32-membered macrocyclic rings in the coordination networks of **1** and **2**, formed between two parallel adjacent $[PdCl_2(\text{2-Clnic})_2]^{2-}$ or $[PdBr_2(\text{2-Brnic})_2]^{2-}$ moieties and six water-bridged sodium ions (Figure 2a,b), with the shortest distance between the neighboring palladium(II) ions in this macrocyclic ring of 5.537(2) Å for **1** and 5.573(2) Å for **2**. The coordination networks of **1** and **2** are stacked along the [010] direction and connected in turn by intermolecular O−H···O hydrogen bonds (Figures S17 and S18). These hydrogen bonds are formed between water molecules as proton donors and carboxylate O atoms as proton acceptors (Table S2). The lattice water molecules in **2** are situated in between the adjacent coordination networks, participating in hydrogen bonding as both proton donors and acceptors (Figure S18, Table S2) and giving rise to a more complex hydrogen-bonded framework in **2**, if compared to that in **1**.

Since the palladium(II) ion is placed on an inversion center in both **3** and **4**, the asymmetric units of **3** and **4** are composed of a palladium(II) ion, a coordinated chloride ion, a coordinated 2-chloronicotinic (in **3**) or a 2-bromonicotinic acid molecule (in **4**), and a lattice *N*,*N*′-dimethylformamide molecule (Figure 3a,b). The overlay of the $[PdCl_2(\text{2-ClnicH})_2]$ and $[PdCl_2(\text{2-BrnicH})_2]$ molecules is shown in Figure 3c, with the lattice DMF molecules being omitted. Each of the palladium(II) ions in **3** and **4** is coordinated with two halide ions [Cl1 and $Cl1^{ii}$ (in **3**) or $Cl1^{iii}$ (in **4**)] and two pyridine N atoms [N1 and $N1^{ii}$ (in **3**) or $N1^{iii}$ (in **4**)] in *trans* position [N1−Pd1−$N1^{ii}$, 180° (in **3**) and N1−Pd1−$N1^{iii}$, 180.0(2)° (in **4**); symmetry codes (ii): $-x + 1, -y + 1, -z$ and (iii): $-x + 1, -y + 1, -z + 1$], resulting in a square-planar coordination environment (Figure 3a,b and Table S1) with τ_4 value[47] of 0 for both **3** and **4**. The palladium(II) square-planar coordination environments are again not distorted (Table S1). The square planes around palladium(II) (defined by Cl1/N1/$Cl1^{ii}$/$N1^{ii}$ atoms in **3** or Cl1/N1/$Cl1^{iii}$/$N1^{iii}$ atoms in **4**) are almost perpendicular to the corresponding pyridine rings defined by N1/C1/C2/C3/C4/C5 atoms [71.7(3)° in **3** and 88.1(2)° in **4**]. Each $[PdCl_2(\text{2-ClnicH})_2]$ or $[PdCl_2(\text{2-BrnicH})_2]$ molecule in the crystal packings of **3** and **4** (Figures S19 and S20), respectively, is connected to two lattice DMF molecules by intermolecular O−H···O hydrogen bonds. These hydrogen bonds are formed between carboxylic O atoms as proton donors and DMF O atoms as proton acceptors (Table S2), giving rise to the discrete $D_1^1(14)$ hydrogen bond motif (Figures S19 and S20). The resulting hydrogen-bonded trimers in the crystal packing of **3** are held together only by weak C−H···π interactions [formed between methyl C8 atom and pyridine ring N1/C1/C2/C3/C4/C5 (Cg1); distance C8···Cg1, 3.81(1) Å, angle C8−H8B···Cg1, 147°]. However, the hydrogen-bonded trimers in the crystal packing of **4** are held together by Cl···π interactions [formed between Cl1 atom and pyridine ring N1/C1/C2/C3/C4/C5 (Cg1): distance Cl1···Cg1 3.732(3) Å; angle Pd1−Cl1···Cg1, 162.85(8)°].

The complexes **3** and **4** are similar to the palladium(II) complexes with nicotinic acid, $[PdCl_2(\text{nicH})_2]$[48,49] and $[PdCl_2(\text{nicH})_2]\cdot 2DMSO$.[49] These complexes contain palladium(II) ions, each of them being coordinated with two chloride ions and two nicotinic acid (nicH) molecules (bound in an *N*-monodentate fashion) in *trans* position, but with or without lattice DMSO molecules in the crystal packing. Consequently, in the absence of solvent molecules, the $[PdCl_2(\text{nicH})_2]$ molecules are connected into a 1D supramolecular zigzag chain *via* intermolecular O−H···O hydrogen bonds between carboxylic groups and giving rise to the anticipated $R_2^2(8)$ synthon,[48,49] as opposed to the hydrogen bonding in the crystal packings of **3** and **4**. However, in the presence of lattice DMSO molecules in the respective crystal packing, the $R_2^2(8)$ synthon is disrupted by the presence of the O−H···O hydrogen bonds between carboxylic groups and DMSO molecules,[49] similar to the H-bonding between carboxylic groups and DMF molecules in the crystal packings of **3** and **4**.

The experimental PXRD traces of the bulks of compounds **1**−**4** overlap nicely with the corresponding calculated traces from the single crystal diffraction data, indicating a phase purity of the prepared coordination polymers **1** and **2** and monomers **3** and **4** (Figure 4).

3.3. Thermal Studies. The thermal stability of the compounds **1**−**4** was studied by TGA and DSC methods (Figures S21−S24) in flowing nitrogen. Thermal degradation of compounds begins, as expected, with solvent elimination which starts for compounds **1** and **2** at temperatures slightly above room temperature. The water elimination from the structures of polymers **1** and **2** is characterized by three endothermic signals on DSC curves (76.3, 90.5, and 114.7 °C for **1**, 69.9, 95.3, and 108.1 °C for **2**). The first step on TGA curves of **1** and **2** is connected with a mass loss of 11.87% (**1**)

https://doi.org/10.1021/acsomega.3c09497
ACS Omega 2024, 9, 4111−4122

and 12.05% (**2**), and corresponds to the elimination of water molecules. The observed discrepancy between calculated (16.76% for **1**, 16.78% for **2**) and experimental values can be explained by the partial decomposition of **1** and **2** (caused by water molecules loss) due to the grinding during samples preparation, which initiates the solvent loss from **1** and **2** prior to the actual start of the respective TGA/DSC measurement.

The DSC curves of palladium(II) monomers **3** and **4** show one endothermic signal (134.2 °C for **3** and 134.2 °C for **3**) due to the elimination of the lattice DMF molecules from the crystal structures. The mass losses of 22.25% (calcd 22.88%) and 18.61% (calcd 20.09%), observed at the TGA curve of **3** and **4**, respectively, correspond to the elimination of two DMF molecules. After elimination of solvent molecules, a continuous thermal degradation of compounds **1**−**4** was observed. The corresponding DSC curves reveal one exothermic and one endothermic signal (**1**), one exothermic and two endothermic signals (**2**), and one endothermic signal (**3** and **4**). The total mass losses of 48.24% (**1**), 54.48% (**2**), 69.70% (**3**), and 73.45% (**4**) were observed at 1000 °C.

3.4. Computational Studies. As all 2-halonicotinate/2-halonicotinic acid ligands were *trans*-coordinated to palladium(II) ions in **1**−**4**, first we investigated the effect of *trans vs cis* coordination on the stability of isolated palladium(II) configurational stereoisomers. *Trans* arrangement of ligands around palladium(II) was found to be more favorable by about 10 kJ mol^{-1} in [$PdCl_2$(2-ClnicH)$_2$] and 15 kJ mol^{-1} in [$PdBr_2$(2-BrnicH)$_2$], thus confirming that different halogens (Cl *vs* Br) do not change the preferred *trans* orientation around palladium(II), but only slightly affect the equilibrium of these two configurational stereoisomers (Figure 5).

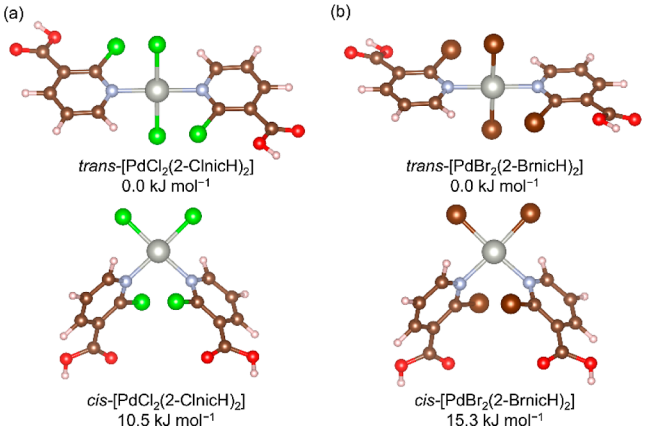

Figure 5. Optimized geometries and relative energies of *trans* and *cis* isomers of [$PdCl_2$(2-ClnicH)$_2$] (a) and [$PdBr_2$(2-BrnicH)$_2$] (b).

A closer look at X-ray-determined crystal structures revealed that [PdX_2(2-Xnic)$_2$]$^{2-}$ moieties are coordinated to sodium ions *via* nicotinates in **1** (X = Cl) and **2** (X = Br), or [$PdCl_2$(2-XnicH)$_2$] hydrogen-bonded to DMF *via* the nicotinic acid carboxylic group in **3** and **4**. In this way, the red-colored regions of the zigzag chains of water-bridged sodium ions separate green-colored regions of [PdX_2(2-Xnic)$_2$]$^{2-}$ moieties in **1** and **2** (Figure 6a,b). In **4**, regions containing water-bridged sodium ions are substituted by DMF molecules organized in a very similar fashion, while **3** has a different arrangement of molecules where both regions are interweaved (compare Figures S7 and S8), and thus structure **3** was excluded from further calculations. To compare the interaction strength between these red/green regions, we have calculated the basis set superposition error (BSSE) corrected interaction energies, E_{int}, by applying the very simple model, $E_{A\cdots B} - (E_A + E_B)$, where $E_{A\cdots B}$ describes the energy of fully optimized unit cell, and E_A and E_B are single point energies of individual fragments with the same geometry and arrangement of molecules as in the optimized unit cell. As expected, the interactions between red/green fragments (Figure 6) are much stronger for negatively charged [PdX_2(2-Xnic)$_2$]$^{2-}$ moieties coordinated to positively charged sodium ions due to high ion−ion attractions in **1** and **2**, than for neutral [$PdCl_2$(2-BrnicH)$_2$] molecules hydrogen-bonded to DMF in **4**.

Next, we investigated the effect of the lattice water molecules, found in the crystal structure of **2** but not of **1**, on the interactions between the zigzag chains. We have calculated the E_{int} between the directly connected zigzag chains (colored red and green in Figure 7a) in the experimentally characterized **1** and in its hypothetical analog, in which Br replaces Cl, labeled as $\mathbf{1}_{Br}$. Because of the slightly larger Br, this substitution increased the Pd···Pd distances (as shown in Figure 7a) and simultaneously strengthened the interactions between the zigzag chains for about 10 kJ mol^{-1}. By including the lattice water molecules between the solvated sodium ions in **2** (and $\mathbf{2}_{Cl}$), two zigzag chains became separated more than they were in **1** (and $\mathbf{1}_{Br}$), but now the interchain Pd···Pd distance was independent of coordinated halogens (about 8.04 Å, as shown in Figure 3b). The introduction of lattice water molecules resulted in stronger interactions between the three fragments, both zigzag chains (colored red and green) and two water molecules (colored blue). In both investigated systems, without lattice water molecules (**1** and $\mathbf{1}_{Br}$) and with them (**2** and $\mathbf{2}_{Cl}$), interactions in Br-containing compounds were found to be stronger. Although we did not experimentally confirm the existence of $\mathbf{2}_{Cl}$, which is suggested by the computational study, a possible explanation can be found in the calculated ΔE_{int} values. The lattice water molecules make the interaction energies more negative (for about 18 kJ mol^{-1}) in case Br are coordinated to palladium(II) and as a part of 2-halonicotinates. The calculated E_{int} value (Figure S25) is the additional evidence that the lattice water molecules keep the two zigzag chains further apart in **2** (and $\mathbf{2}_{Cl}$), compared to **1** (and $\mathbf{1}_{Br}$), weakening their direct interactions. If the water molecules had not been included in E_{int} calculations of **2** (and $\mathbf{2}_{Cl}$), we obtained less negative values of E_{int} (weaker interaction) for the almost identical arrangement of molecules as in **1** (and $\mathbf{1}_{Cl}$).

3.5. Biological Activity. The antimicrobial activity of the compounds **1**−**4** was assessed against reference strains of *E. coli* and *S. aureus*. From the data, it can be concluded that the compounds have very weak or no antibacterial activity, as the MIC was higher than the highest compound concentration used for testing (MIC > 128 μg mL^{-1}).

The antiproliferative activity of the tested compounds **1**−**4** was determined on bladder and lung cancer cell lines, T24 and A549, respectively. All compounds showed very weak or no effect on both cell lines (Figures S26 and S27). The IC_{50} values could not be determined for the majority of samples, except for **1** on A549 cell line (IC_{50} after 72 h was 69.65 μg mL^{-1}).

4. CONCLUSIONS

We have shown that the heterometallic sodium−palladium(II) coordination polymers **1** and **2** can be indeed prepared by

https://doi.org/10.1021/acsomega.3c09497
ACS Omega 2024, 9, 4111−4122

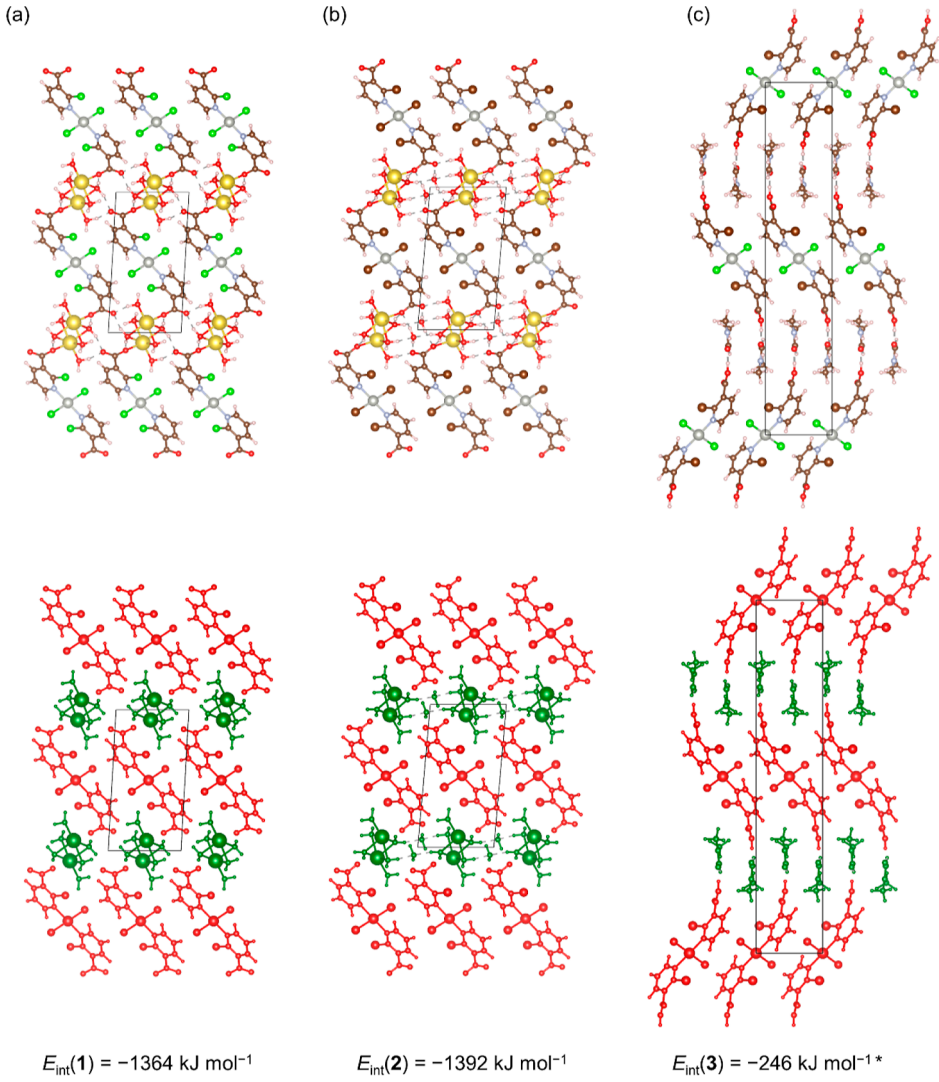

Figure 6. BSSE-corrected interaction energies (PBE-D3/pob-TZVP-rev2) per unit cell [and per one palladium(II) center in **4***] calculated between $[PdX_2(2\text{-Xnic})_2]^{2-}$ moieties (red) and water-bridged sodium ions regions (green) in **1** (a) and **2** (b), and between $[PdCl_2(2\text{-BrnicH})_2]$ (red) and lattice DMF molecules (green) in **4** (c).

employing 2-halonicotinates as bridging ligands between palladium(II) and sodium ions. The 2-halonicotinates coordinate to palladium(II) ions *via* their N atoms in a monodentate fashion and to sodium ions *via* their carboxylate O atoms, leading to a square-planar coordination environment around palladium(II) ions, completed with halide ions, as anticipated. However, such palladium(II) coordination environments in **1** and **2** are not the same as in the related sodium− and potassium−palladium(II) coordination polymers with pyridine-2,6-dicarboxylate[32] and pyridine-2,3-dicarboxylate,[33] respectively, because of the pyridinedicarboxylates *N*,*O*-bidentate coordination mode. Furthermore, the coordination polymers **1** and **2** can be formed only in the aqueous solution in the presence of the base (sodium bicarbonate), as the deprotonation of the carboxylic groups and presence of carboxylate is crucial for their formation. The carboxylate O atoms are able to coordinate to sodium ions leading to the formation of 2D coordination networks. On the contrary, the carboxylic groups are not deprotonated in the DMF/water mixture. Hence, the carboxylic O atoms cannot coordinate to sodium ions, leading to the formation of simple palladium(II) monomers **3** and **4**, which are further stabilized by O−H···O hydrogen bonds between carboxylic groups and DMF molecules. According to DFT calculations, the 2D coordination networks **1** and **2** are way more stabilized by the formation of $Na-O_{carboxylate}$ bonds, comparing to the stabilization of palladium(II) monomers **3** and **4** offered by O−H···O hydrogen-bonding with DMF molecules. Furthermore, we have shown that the choice of halosubstituents (Cl or Br) in the position 2- on the pyridine ring does not have any influence on either formation or dimensionality of the obtained coordination polymers. The analogous 2D polymers were obtained by employing either 2-choronicotinate or 2-bromonicotonate, but only in water solution in the presence of the base. Also, the halosubstituents type definitely does not have any influence on the formation of either *trans* or *cis* arrangement around palladium(II) ions, as the *trans* isomers were exclusively found in all reported coordination polymers and monomers (being more stable for about 10 to 15 kJ mol^{-1}). Finally, the difference in DFT calculated energy stabilization for polymers **1** and **2** should be ascribed to the type of halosubstituents and to the presence/absence of lattice water molecules in polymers **1** and **2**.

https://doi.org/10.1021/acsomega.3c09497
ACS Omega 2024, 9, 4111−4122

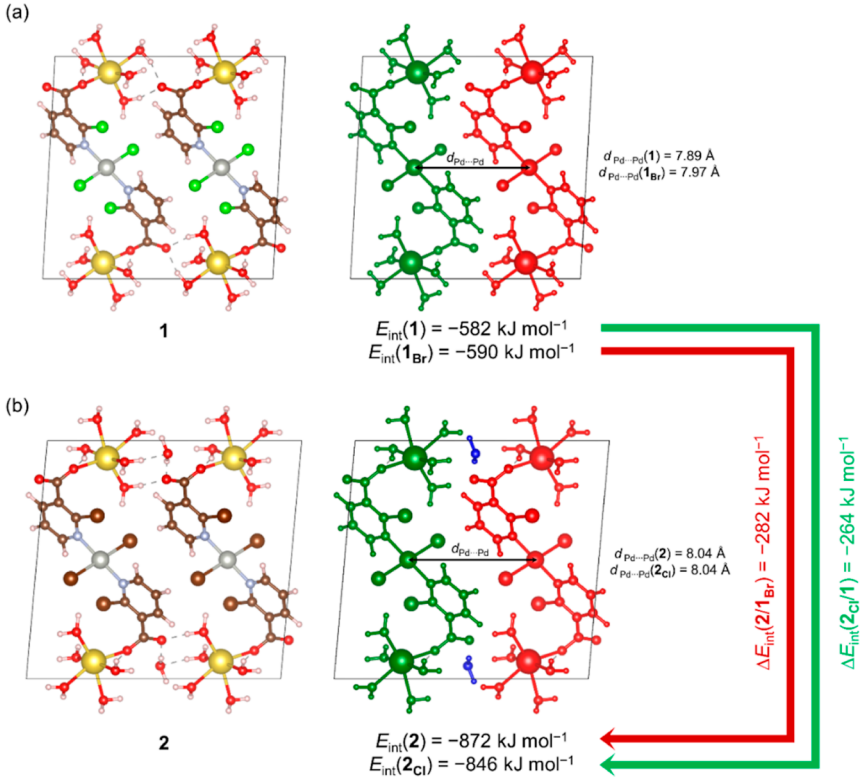

Figure 7. BSSE-corrected interaction energies (PBE-D3/pob-TZVP-rev2) calculated for (a) two fragments (red and green) in the unit supercells of real model **1** and its hypothetical analog $\mathbf{1}_{Br}$ and (b) between three fragments (red, green and blue) in the unit supercells of real model **2** and its hypothetical analog $\mathbf{2}_{Cl}$. The calculated ΔE_{int} shows a larger stabilization for Br compared to Cl.

■ ASSOCIATED CONTENT

Supporting Information

The Supporting Information is available free of charge at https://pubs.acs.org/doi/10.1021/acsomega.3c09497.

IR spectra of **1**−**4**; ^{1}H NMR spectra of free ligands and **1**−**4**; ^{13}C NMR spectra of free ligands and **1**−**4**; a view of the crystal packings of **1** and **2**, respectively, down the [100] direction; a view of the crystal packings of **3** and **4**, respectively, down the [100] direction; TGA/DSC curves of **1**−**4**; BSSE-corrected interaction energies (PBE-D3/pob-TZVP-rev2) calculated for two fragments in the unit supercells of the real model **2** and its hypothetical analog $\mathbf{2}_{Cl}$; bladder cancer (T24) and lung cancer (A549) cell viabilities, respectively, after treatment with compounds **1**−**4**; selected bond lengths (Å) and angles (deg) for **1**−**4**; and the hydrogen bond geometry for **1**−**4** (PDF)

CIF file of **1** (CIF)

CIF file of **2** (CIF)

CIF file of **3** (CIF)

CIF file of **4** (CIF)

Accession Codes

CCDC 2291904−2291907 for **1**−**4** contain the supplementary crystallographic data for this paper. These data can be obtained free of charge *via* www.ccdc.cam.ac.uk/data_request/cif, or by emailing data_request@ccdc.cam.ac.uk, or by contacting The Cambridge Crystallographic Data Centre, 12 Union Road, Cambridge CB21EZ, UK; fax: +441223336033.

■ AUTHOR INFORMATION

Corresponding Authors

Fabio Doctorovich − *INQUIMAE-CONICET; DQIAQF-FCEyN, Universidad de Buenos Aires, C1428EGA Buenos Aires, Argentina;* orcid.org/0000-0003-1088-2089; Email: doctorovich@qi.fcen.uba.ar

Boris-Marko Kukovec − *Department of Physical Chemistry, Faculty of Chemistry and Technology, University of Split, HR-21000 Split, Croatia;* orcid.org/0000-0002-9582-404X; Email: bmkukovec@ktf-split.hr

Authors

Ivan Kodrin − *Department of Chemistry, Faculty of Science, University of Zagreb, HR-10000 Zagreb, Croatia;* orcid.org/0000-0001-6353-3187

Maricel Rodríguez − *INQUIMAE-CONICET; DQIAQF-FCEyN, Universidad de Buenos Aires, C1428EGA Buenos Aires, Argentina*

Nives Politeo − *Department of Physical Chemistry, Faculty of Chemistry and Technology, University of Split, HR-21000 Split, Croatia*

Željka Soldin − *Department of Chemistry, Faculty of Science, University of Zagreb, HR-10000 Zagreb, Croatia;* orcid.org/0000-0003-4206-8209

Igor Kerš − *Department of Chemistry, Faculty of Science, University of Zagreb, HR-10000 Zagreb, Croatia*

Tomislav Rončević − *Department of Biology, Faculty of Science, University of Split, HR-21000 Split, Croatia;* orcid.org/0000-0002-6426-6655

Vedrana Čikeš Čulić − *School of Medicine, University of Split, HR-21000 Split, Croatia*

https://doi.org/10.1021/acsomega.3c09497
ACS Omega 2024, 9, 4111−4122

Vesna Sokol − *Department of Physical Chemistry, Faculty of Chemistry and Technology, University of Split, HR-21000 Split, Croatia*

Complete contact information is available at: https://pubs.acs.org/10.1021/acsomega.3c09497

Author Contributions

The manuscript was written through contributions of all authors. All authors have given approval to the final version of the manuscript.

Notes

The authors declare no competing financial interest.

■ ACKNOWLEDGMENTS

This work was supported by the Faculty of Chemistry and Technology, University of Split (institutional funds awarded to V.S. and B.-M.K.), by the Foundation of the Croatian Academy of Sciences and Arts (grants awarded to I.K. and B.-M.K.), and by the European Regional Development Fund [infrastructural project CIuK (KK.01.1.1.02.0016)]. We thank Assoc. Prof. Ivana Biljan for the help with the NMR analysis.

■ REFERENCES

(1) Abu-Surrah, A. S.; Kettunen, M. Platinum Group Antitumor Chemistry: Design and Development of New Anticancer Drugs Complementary to Cisplatin. *Curr. Med. Chem.* **2006**, *13*, 1337−1357.
(2) Bruijnincx, P. C. A.; Sadler, P. J. New Trends for Metal Complexes with Anticancer Activity. *Curr. Opin. Chem. Biol.* **2008**, *12*, 197−206.
(3) Ćoćić, D.; Jovanović-Stević, S.; Jelić, R.; Matić, S.; Popović, S.; Djurdjević, P.; Baskić, D.; Petrović, B. Homo- and Hetero-Dinuclear Pt(II)/Pd(II) Complexes: Studies of Hydrolysis, Nucleophilic Substitution Reactions, DNA/BSA Interactions, DFT Calculations, Molecular Docking and Cytotoxic Activity. *Dalton Trans.* **2020**, *49*, 14411−14431.
(4) Shoukry, M. M.; van Eldik, R. Equilibrium Studies on Pd(II)-Amine Complexes with Bio-Relevant Ligands in Reference to Their Antitumor Activity. *Int. J. Mol. Sci.* **2023**, *24*, 4843.
(5) Rau, T.; Eldik, R. V. Mechanistic Insight from Kinetic Studies on the Interaction of Model Palladium(II) Complexes with Nucleic Acid Components. *Met. Ions Biol. Syst.* **1996**, *32*, 339−378.
(6) Saygıdeğer Demir, B.; Ince, S.; Yilmaz, M. K.; Sezan, A.; Derinöz, E.; Taskin-Tok, T.; Saygideger, Y. DNA Binding and Anticancer Properties of New Pd(II)-Phosphorus Schiff Base Metal Complexes. *Pharmaceutics* **2022**, *14*, 2409.
(7) Kuwamura, N.; Konno, T. Heterometallic Coordination Polymers as Heterogeneous Electrocatalysts. *Inorg. Chem. Front.* **2021**, *8*, 2634−2649.
(8) Andruh, M. Heterotrimetallic Complexes in Molecular Magnetism. *Chem. Commun.* **2018**, *54*, 3559−3577.
(9) Zhang, W.-H.; Liu, Q.; Lang, J.-P. Heterometallic Transition Metal Clusters and Cluster-Supported Coordination Polymers Derived from Tp- and Tp*-Based Mo(W) Sulfido Precursors. *Coord. Chem. Rev.* **2015**, *293*−*294*, 187−210.
(10) Andruh, M.; Costes, J.-P.; Diaz, C.; Gao, S. 3*d*-4*f* Combined Chemistry: Synthetic Strategies and Magnetic Properties. *Inorg. Chem.* **2009**, *48*, 3342−3359.
(11) Zhang, S.; Cheng, P. Recent Advances in the Construction of Lanthanide-Copper Heterometallic Metal-Organic frameworks. *CrystEngComm* **2015**, *17*, 4250−4271.
(12) Cahill, C. L.; de Lill, D. T.; Frisch, M. Homo- and Heterometallic Coordination Polymers from the *f* Elements. *CrystEngComm* **2007**, *9*, 15−26.
(13) Goetjen, T. A.; Liu, J.; Wu, Y.; Sui, J.; Zhang, X.; Hupp, J. T.; Farha, O. K. Metal-Organic Framework (MOF) Materials as Polymerization Catalysts: a Review and Recent Advances. *Chem. Commun.* **2020**, *56*, 10409−10418.
(14) Wang, Q.; Astruc, D. State of the Art and Prospects in Metal-Organic Framework (MOF)-Based and MOF-Derived Nanocatalysis. *Chem. Rev.* **2020**, *120*, 1438−1511.
(15) Chorazy, S.; Wyczesany, M.; Sieklucka, B. Lanthanide Photoluminescence in Heterometallic Polycyanidometallate-Based Coordination Networks. *Molecules* **2017**, *22*, 1902.
(16) Liao, P.-Q.; Shen, J.-Q.; Zhang, J.-P. Metal-Organic Frameworks for Electrocatalysis. *Coord. Chem. Rev.* **2018**, *373*, 22−48.
(17) Biradha, K.; Goswami, A.; Moi, R. Coordination Polymers as Heterogeneous Catalysts in Hydrogen Evolution and Oxygen Evolution Reactions. *Chem. Commun.* **2020**, *56*, 10824−10842.
(18) Zhang, H.; Su, J.; Zhao, K.; Chen, L. Recent Advances in Metal-Organic Frameworks and Their Derived Materials for Electrocatalytic Water Splitting. *ChemElectroChem* **2020**, *7*, 1805−1824.
(19) Wang, W.; Xu, X.; Zhou, W.; Shao, Z. Recent Progress in Metal-Organic Frameworks for Applications in Electrocatalytic and Photocatalytic Water Splitting. *Adv. Sci.* **2017**, *4*, 1600371.
(20) Mukhopadhyay, S.; Basu, O.; Nasani, R.; Das, S. K. Evolution of Metal-Organic Frameworks as Electrocatalysts for Water Oxidation. *Chem. Commun.* **2020**, *56*, 11735−11748.
(21) Budnikova, Y. H. Recent Advances in Metal-Organic Frameworks for Electrocatalytic Hydrogen Evolution and Overall Water Splitting Reactions. *Dalton Trans.* **2020**, *49*, 12483−12502.
(22) Zheng, F.; Zhang, Z.; Zhang, C.; Chen, W. Advanced Electrocatalysts Based on Metal-Organic Frameworks. *ACS Omega* **2020**, *5*, 2495−2502.
(23) Zhu, D.; Qiao, M.; Liu, J.; Tao, T.; Guo, C. Engineering Pristine 2D Metal-Organic Framework Nanosheets for Electrocatalysis. *J. Mater. Chem. A* **2020**, *8*, 8143−8170.
(24) Xue, J. Y.; Li, C.; Li, F. L.; Gu, H.-W.; Braunstein, P.; Lang, J.-P. Recent Advances in Pristine Tri-Metallic Metal−Organic Frameworks toward the Oxygen Evolution Reaction. *Nanoscale* **2020**, *12*, 4816−4825.
(25) Fortea-Pérez, F. R.; Mon, M.; Ferrando-Soria, J.; Boronat, M.; Leyva-Pérez, A.; Corma, A.; Herrera, J. M.; Osadchii, D.; Gascon, J.; Armentano, D.; Pardo, E. The MOF-Driven Synthesis of Supported Palladium Clusters with Catalytic Activity for Carbene-Mediated Chemistry. *Nat. Mater.* **2017**, *16*, 760−766.
(26) Chen, L.; Gao, Z.; Li, Y. Immobilization of Pd(II) on MOFs as a Highly Active Heterogeneous Catalyst for Suzuki-Miyaura and Ullmann-Type Coupling Reactions. *Catal. Today* **2015**, *245*, 122−128.
(27) Miguel-Casañ, E.; Darawsheh, M. D.; Fariña-Torres, V.; Vitórica-Yrezábal, I. J.; Andres-Garcia, E.; Fañanás-Mastral, M.; Mínguez Espallargas, G. Heterometallic Palladium-Iron Metal-Organic Framework as a Highly Active Catalyst for Cross-Coupling Reactions. *Chem. Sci.* **2023**, *14*, 179−185.
(28) Androš, L.; Jurić, M.; Popović, J.; Pajić, D.; Zadro, K.; Molčanov, K.; Žilić, D.; Planinić, P. 1D Heterometallic Oxalate Compounds as Precursors for Mixed Ca-Cr Oxides - Synthesis, Structures, and Magnetic Studies. *Eur. J. Inorg. Chem.* **2014**, *2014*, 5703−5713.
(29) Habjanič, J.; Jurić, M.; Popović, J.; Molčanov, K.; Pajić, D. A 3D Oxalate-Based Network as a Precursor for the $CoMn_2O_4$ Spinel: Synthesis and Structural and Magnetic Studies. *Inorg. Chem.* **2014**, *53*, 9633−9643.
(30) Molčanov, L.; Androš Dubraja, L.; Vrankić, M.; Jurić, M. A 3D Oxalate-Bridged $[Cu^{II}Fe^{II}]$ Coordination Polymer as Molecular Precursor for $CuFe_2O_4$ Spinel - Photocatalytic Features. *J. Am. Ceram. Soc.* **2023**, *106*, 2997−3008.
(31) Smrečki, N.; Kukovec, B.-M.; Rotim, K.; Oršolić, D.; Jović, O.; Rončević, T.; Mužinić, N. R.; Vinković, M.; Popović, Z. Palladium(II) Complexes with *N*-Alkyliminodiacetic Acid Derivatives: Preparation, Structural and Spectroscopic Studies. *Inorg. Chim. Acta* **2017**, *462*, 64−74.
(32) Chakraborty, J.; Mayer-Figge, H.; Sheldrick, W. S.; Banerjee, P. Structure and Property of Unsymmetrical Binuclear [(3,5-Dimethyl-

https://doi.org/10.1021/acsomega.3c09497
ACS Omega 2024, 9, 4111−4122

pyrazole)$_2$Pd$_2$(μ-3,5-Dimethylpyrazolate)$_2$(2,6-Dipicolinate)] and Mononuclear [Na$_2$(H$_2$O)$_4$Pd(2,6-Dipicolinate)$_2$] Complexes. *Polyhedron* **2006**, *25*, 3138−3144.
(33) Gao, E.-J.; Zhu, M.-C.; Huang, Y.; Liu, L.; Liu, H.-Y.; Liu, F.-C.; Ma, S.; Shi, C.-Y. New pH-Dependent Complexes, from Mononuclear Pd(II) Monomer to Heteronuclear [Pd(II),K(I)] Polymer: DNA Cleavage and Cytotoxicity in Vitro. *Eur. J. Med. Chem.* **2010**, *45*, 1034−1041.
(34) Pearson, R. G. Hard and Soft Acids and Bases. *J. Am. Chem. Soc.* **1963**, *85*, 3533−3539.
(35) *CrysAlis PRO*; Rigaku Oxford Diffraction Ltd: Yarnton, Oxfordshire, England, 2021.
(36) Sheldrick, G. M. *SHELXT* - Integrated Space-Group and Crystal-Structure Determination. *Acta Crystallogr., Sect. A: Found. Adv.* **2015**, *71*, 3−8.
(37) Sheldrick, G. M. Crystal Structure Refinement with *SHELXL*. *Acta Crystallogr., Sect. C: Struct. Chem.* **2015**, *71*, 3−8.
(38) Macrae, C. F.; Sovago, I.; Cottrell, S. J.; Galek, P. T. A.; McCabe, P.; Pidcock, E.; Platings, M.; Shields, G. P.; Stevens, J. S.; Towler, M.; Wood, P. A. *Mercury 4.0*: from Visualization to Analysis, Design and Prediction. *J. Appl. Crystallogr.* **2020**, *53*, 226−235.
(39) Dovesi, R.; Erba, A.; Orlando, R.; Zicovich-Wilson, C. M.; Civalleri, B.; Maschio, L.; Rérat, M.; Casassa, S.; Baima, J.; Salustro, S.; Kirtman, B. Quantum-Mechanical Condensed Matter Simulations with CRYSTAL. *Wiley Interdiscip. Rev.: Comput. Mol. Sci.* **2018**, *8*, No. e1360.
(40) Perdew, J. P.; Chevary, J. A.; Vosko, S. H.; Jackson, K. A.; Pederson, M. R.; Singh, D. J.; Fiolhais, C. Atoms, Molecules, Solids, and Surfaces: Applications of the Generalized Gradient Approximation for Exchange and Correlation. *Phys. Rev. B* **1992**, *46*, 6671−6687.
(41) Grimme, S.; Antony, J.; Ehrlich, S.; Krieg, H. A Consistent and Accurate *ab Initio* Parametrization of Density Functional Dispersion Correction (DFT-D) for the 94 Elements H-Pu. *J. Chem. Phys.* **2010**, *132*, 154104.
(42) Vilela Oliveira, D.; Laun, J.; Peintinger, M. F.; Bredow, T. BSSE-Correction Scheme for Consistent Gaussian Basis Sets of Double- and Triple-Zeta Valence with Polarization Quality for Solid-State Calculations. *J. Comput. Chem.* **2019**, *40*, 2364−2376.
(43) Björkman, T. CIF2Cell: Generating Geometries for Electronic Structure Programs. *Comput. Phys. Commun.* **2011**, *182*, 1183−1186.
(44) Momma, K.; Izumi, F. *VESTA 3* for Three-Dimensional Visualization of Crystal, Volumetric and Morphology Data. *J. Appl. Crystallogr.* **2011**, *44*, 1272−1276.
(45) Boys, S. F.; Bernardi, F. The Calculation of Small Molecular Interactions by the Differences of Separate Total Energies. Some Procedures with Reduced Errors. *Mol. Phys.* **1970**, *19*, 553−566.
(46) Rončević, T.; Gerdol, M.; Mardirossian, M.; Maleš, M.; Cvjetan, S.; Benincasa, M.; Maravić, A.; Gajski, G.; Krce, L.; Aviani, I.; Hrabar, J.; Trumbić, Ž.; Derks, M.; Pallavicini, A.; Weingarth, M.; Zoranić, L.; Tossi, A.; Mladineo, I. Anisaxins, Helical Antimicrobial Peptides from Marine Parasites, Kill Resistant Bacteria by Lipid Extraction and Membrane Disruption. *Acta Biomater.* **2022**, *146*, 131−144.
(47) Yang, L.; Powell, D. R.; Houser, R. P. Structural Variation in Copper(i) Complexes with Pyridylmethylamide Ligands: Structural Analysis with a New Four-Coordinate Geometry Index, τ_4. *Dalton Trans.* **2007**, 955−964.
(48) Qin, Z.; Jenkins, H. A.; Coles, S. J.; Muir, K. W.; Puddephatt, R. J. Self-Assembly of One-Dimensional Polymers by Coordination and Hydrogen Bonding in Palladium(II) Complexes. *Can. J. Chem.* **1999**, *77*, 155−157.
(49) Qin, Z.; Jennings, M. C.; Puddephatt, R. J.; Muir, K. W. Self-Assembly of Polymer and Sheet Structures in Palladium(II) Complexes Containing Carboxylic Acid Substituents. *Inorg. Chem.* **2002**, *41*, 5174−5186.

https://doi.org/10.1021/acsomega.3c09497
ACS Omega 2024, 9, 4111−4122